Journal of Sound and Vibration 330 (2011) 567–580

Contents lists available at ScienceDirect

Journal of Sound and Vibration

journal homepage: www.elsevier.com/locate/jsvi

Three dimensional vibration generators with a single rotational input

Shang-Teh Wu *

Department of Mechanical Engineering, National Yunlin University of Science & Technology, Touliu, Yunlin 640, Taiwan

ARTICLE INFO

Article history:
Received 5 March 2010
Received in revised form
1 July 2010
Accepted 22 August 2010
Handling Editor: L.G. Tham
Available online 9 September 2010

ABSTRACT

This paper presents a novel device capable of generating three-dimensional vibrations with a single-axis of rotation. The device resembles a vibration motor with an eccentric weight, but the weight is allowed to move up and down in parallel to the axis of rotations. While spinning of the eccentric weight causes lateral vibrations, vertical vibrations are excited by superposing a periodic torque on the rotary shaft. The frequency and magnitude of vertical oscillations can be independently regulated. Since the vertical natural frequency is sensitive to rotational speeds, maximum vertical oscillations can be achieved by properly adjusting the rotational speed according to the excitation frequency. Relations between the excitation torque and the vertical shaking force are examined using the frequency response for the linearized system. Numerical simulations on the original nonlinear system are conducted to verify the performance of vertical oscillations.

1. Introduction

Vibration generators such as vibration motors or shakers have been found in various applications for the laboratories, the industry, and in commercial products. For example, mobile phones use vibration motors to generate the silent ring tone. In haptic technology, which exploits the sense of touch for tactile feedback, *vibrotactile* devices are used as mechanical stimuli to enhance the sense of existence of virtual parts or remote motions [1–4]. Vibrotactile stimulation is also a tool in neurophysiological research [5]. In industry, vibratory feeders are commonly used in automatic assembly lines for parts conveyance and alignment [6–9], and other similar applications such as food packaging, precision mixing of chemical and pharmaceutical ingredients, or material conveying for mineral processing [10].

The vibration motor is a simple electric motor with an eccentric weight; when turning it generates circular oscillations. Directional vibrations can be produced by a linear actuator such as a voice-coil motor, which operates around its natural frequency determined by the shaft's inertia and an installed spring [2,4]. For vibratory bowl feeders, however, neither an eccentric-weight vibration motor nor a linear voice-coil motor is adequate because the required vibrations are spiral, that is, a combination of circular and linear (up and down) oscillations. That is why a bowl feeder utilizes rather complicated mechanism to produce the helical vibrations [11]. The sophisticated velocity fields in the bowl feeders were also investigated in the literature [7,12,13]. As an alternative to electromagnet-based actuators used in conventional vibratory feeders, piezoelectric actuators were explored to simplify mechanism design and improve the dynamic response [14,15].

This paper presents a novel mechanism that is capable of generating vertical and horizontal oscillations simultaneously. The device resembles a vibration motor with an extra degree of freedom for the eccentric weight, which is allowed to move

* Tel.: +886 5 5342601 4111; fax: 886 5 5312062.
E-mail address: wust@yuntech.edu.tw

0022-460X/$ - see front matter © 2010 Elsevier Ltd. All rights reserved.
doi:10.1016/j.jsv.2010.08.029

up and down freely in parallel to the axis of rotations. While lateral vibrations are generated by turning the weight at a desired speed, axial vibrations can be excited by applying a periodically varying torque to the rotary shaft. It is thus possible to produce oscillations of 3-D patterns, such as a spiral, with this single-input device. In addition, both the frequency and amplitude of axial oscillations can be independently controlled by separately setting the frequency and peak-to-peak value of the input signal. The device is inspired by the rotational-pendulum vibration absorber presented in [16], and can be seen as a reverse mechanism of the vibration absorber. While the frequency of vertical oscillations is determined by the excitation frequency, the magnitude is sensitive to the rotational speed. This is because the natural frequency for vertical motion is dependent on the rotational speed. This vibration generator may thus operate effectively over a wide range of frequencies by varying the rotational speed accordingly.

In the next section the 3-D vibration generator will be introduced. The nonlinear dynamic equations are derived using Lagrange's equations. Relationship between the excitation torque and the vertical shaking force is analyzed in Section 3 by studying the frequency response for the linearized system. In Section 4 numerical simulations on the original nonlinear system are conducted to verify the performance of vertical oscillations. Concluding remarks are given in Section 5.

2. 3-D vibration generator

Fig. 1 compares the construction of a vibratory motor and that of the proposed 3-D vibration generator. The rotational arm of Fig. 1b is allowed to move freely up and down in parallel to the axis of rotation. The arm's rotation generates periodic forces in the lateral directions (F_X and F_Y in Fig. 2). By superposing a periodic signal onto the torque that maintains the arm at a target speed, one may disturb the rotational speed and excite vertical oscillations for the revolving arm. An axial shaking force is thus generated as indicated by F_Z in Fig. 2. Since the lateral forces are a direct result of the rotation

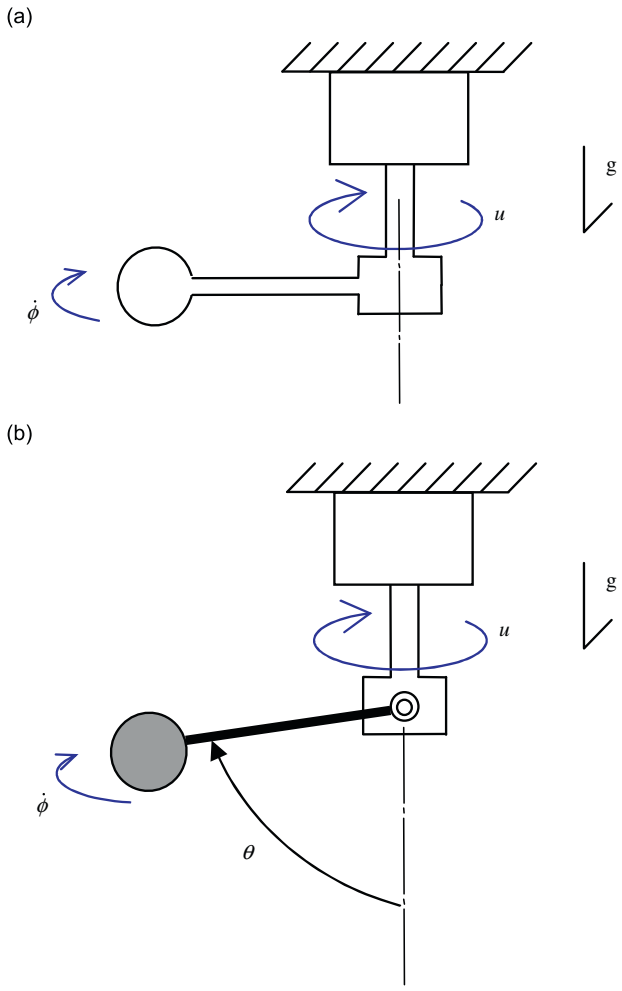

Fig. 1. Schematic comparison of a conventional vibration motor (a) and the proposed 3-D vibration generator (b); the rotational arm in the 3-D generator has an additional freedom of motion.

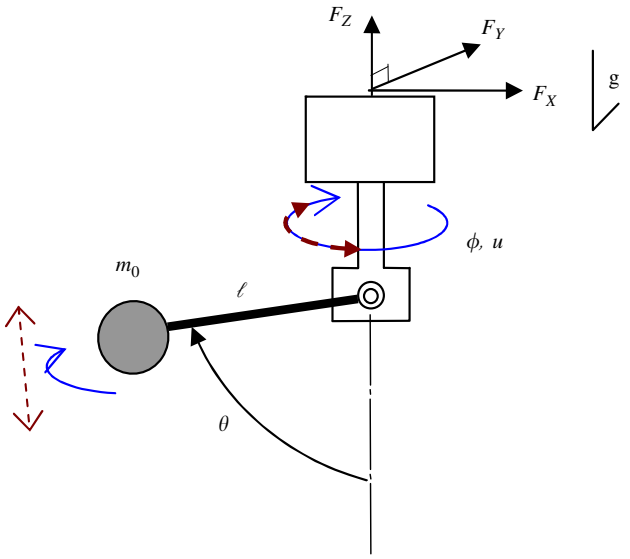

Fig. 2. Free body diagram for the 3-D vibration generator. The rotational arm would oscillate up and down when a periodic torque is superposed on the rotary shaft.

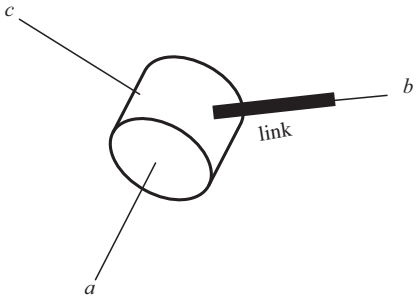

Fig. 3. Three axes for the moment of inertia.

and are self-evident, we will focus on the issue of how to excite the vertical oscillations in a way that the axial force can be effectively generated.

The governing equations for the 3-D vibration generator will be derived using Lagrange's equation. From Fig. 1b, the kinetic and potential energy of the system are, respectively, obtained to be

$$T = \tfrac{1}{2} m_0[\ell^2\dot{\theta}^2 + (\ell\dot{\phi}\sin\theta)^2] + \tfrac{1}{2}(J_a\dot{\theta}^2 + J_b(\dot{\phi}\cos\theta)^2 + J_c(\dot{\phi}\sin\theta)^2), \tag{1}$$

$$V = m_0 g\ell(1-\cos\theta), \tag{2}$$

where θ is the vertical angle of the rotational arm, $\dot{\phi}$ is the angular speed of rotation, m_0 is the mass of the arm, ℓ is the length of the arm measured from the hinge to the center of mass. As illustrated in Fig. 3, J_a is the moment of inertia about the axis passing through the center of mass, perpendicular to both the link (connecting the hinge and the center of mass) and the vertical line; J_b is the moment of inertia about the axis going through the link, and J_c is about the third Cartesian coordinate axis.

Let $\mathcal{L} = T - V$. From

$$\frac{\mathrm{d}}{\mathrm{d}t}\left(\frac{\partial\mathcal{L}}{\partial\dot{\theta}}\right) - \frac{\partial\mathcal{L}}{\partial\theta} = -b_0\dot{\theta}, \tag{3}$$

where b_0 is the damping coefficient for vertical motions, we have

$$(m_0\ell^2 + J_a)\ddot{\theta} + m_0\ell g\sin\theta - \tfrac{1}{2}(m_0\ell^2 + J_c - J_b)\dot{\phi}^2\sin 2\theta = -b_0\dot{\theta}. \tag{4}$$

From

$$\frac{\mathrm{d}}{\mathrm{d}t}\left(\frac{\partial\mathcal{L}}{\partial\dot{\phi}}\right) - \frac{\partial\mathcal{L}}{\partial\phi} = u - b_1\dot{\phi}, \tag{5}$$

where u is the torque applied to the shaft of rotation and b_1 is the rotational damping coefficient, we have

$$(m_0\ell^2+J_c)(\ddot{\phi}\sin^2\theta+\dot{\phi}\dot{\theta}\sin2\theta)+J_b(\ddot{\phi}\cos^2\theta-\dot{\phi}\dot{\theta}\sin2\theta)=u-b_1\dot{\phi}. \tag{6}$$

To simplify the analysis, in what follows the arm is assumed to be a solid spherical body connected by a massless link to the spinning shaft. The mass of the solid ball is m_0 and the radius is r, and ℓ is now the distance from the hinge to the center of the ball. For the moment of inertia, we have $J_a=J_b=J_c=\frac{2}{5}m_0r^2$. Eqs. (4) and (6) can thus be expressed to be

$$m_0(\ell^2+\tfrac{2}{5}r^2)\ddot{\theta}+m_0\ell g\sin\theta-\tfrac{1}{2}m_0\ell^2\dot{\phi}^2\sin2\theta+b_0\dot{\theta}=0, \tag{7}$$

$$m_0\ell^2(\ddot{\phi}\sin^2\theta+\dot{\phi}\dot{\theta}\sin2\theta)+\tfrac{2}{5}m_0r^2\ddot{\phi}+b_1\dot{\phi}=u. \tag{8}$$

Equilibrium angles: The equilibrium vertical angle θ_0 given a constant rotational speed ω_0 can be determined by setting $\ddot{\theta}=\dot{\theta}=0$, $\theta=\theta_0$ and $\dot{\phi}=\omega_0$ in Eq. (7):

$$m_0\ell g\sin\theta_0-\tfrac{1}{2}m_0\ell^2\omega_0^2\sin2\theta_0=0. \tag{9}$$

From Eq. (9), we have

$$\sin\theta_0=0 \tag{10}$$

or

$$\ell\omega_0^2\cos\theta_0=g. \tag{11}$$

A nonzero equilibrium angle can be solved from Eq. (11) to be

$$\theta_0=\cos^{-1}\frac{g}{\ell\omega_0^2}, \tag{12}$$

provided that

$$\omega_0>\sqrt{\frac{g}{\ell}} \tag{13}$$

Physically, Eq. (13) means that, in order to reach a nonzero equilibrium angle, the angular speed must be larger than the radian natural frequency of a corresponding simple pendulum. Since the frequency of lateral oscillations is determined by the rotational speed, the length of the rotational arm should be chosen according to the desired frequency range: The lower the frequencies, the longer the length of arm. Furthermore, it will be shown in the next section that, given an excitation torque, the magnitude of vertical vibrations is sensitive to the rotational speed.

3. Frequency response for vertical oscillations

The relation between a periodic excitation torque on the shaft and vertical oscillations will be studied by examining the frequency response of the system. For this purpose the nonlinear equations of Eqs. (7) and (8) are first linearized about the equilibrium angle ($\theta=\theta_0$) corresponding to a rotational speed ω_0 that is larger than $\sqrt{g/\ell}$. The input variable will be a harmonic torque superposed on the constant level that maintains the spinning arm at a constant speed, and the output variable will be the axial periodic force exerted on the support (F_Z) resulted from vertical oscillations of the arm.

Linearization about the equilibrium angle and speed: Denote the deviations about the equilibrium associated with θ, $\dot{\phi}$ and u to be, respectively, q, p and v such that

$$\theta=\theta_0+q, \tag{14}$$

$$\dot{\phi}=\omega_0+p, \tag{15}$$

$$u=u_0+v, \tag{16}$$

where u_0 is the torque required to keep the arm at the constant rotational speed ω_0. From Eq. (8) we have

$$u_0=b_1\omega_0. \tag{17}$$

Substitute Eqs. (14)–(17) into Eqs. (7) and (8) and we have

$$m_0(\ell^2+\tfrac{2}{5}r^2)\ddot{q}+m_0\ell g\sin(\theta_0+q)-\tfrac{1}{2}m_0\ell^2(\omega_0+p)^2\sin2(\theta_0+q)+b_0\dot{q}=0, \tag{18}$$

$$m_0\ell^2(\dot{p}\sin^2(\theta_0+q)+(\omega_0+p)\dot{q}\sin2(\theta_0+q))+\tfrac{2}{5}m_0r^2\dot{p}+b_1(\omega_0+p)=b_1\omega_0+v. \tag{19}$$

The nonlinear terms in Eq. (18) are each expanded to be

$$m_0\ell g\sin(\theta_0+q) = m_0\ell g\sin\theta_0 + m_0\ell g q\cos\theta_0 + \text{H.O.T.}, \tag{20}$$

$$-\tfrac{1}{2}m_0\ell^2(\omega_0+p)^2\sin2(\theta_0+q) = -\tfrac{1}{2}m_0\ell^2(\omega_0^2\sin2\theta_0 + 2\omega_0 p\sin2\theta_0 + \omega_0^2(2q\cos2\theta_0) + \text{H.O.T.}), \tag{21}$$

where H.O.T. denotes terms associated with q^2, p^2, pq and the higher-order products of p and q. From Eq. (9), Eqs. (20) and (21) can be combined to be

$$m_0\ell g\sin(\theta_0+q) - \tfrac{1}{2}m_0\ell^2(\omega_0+p)^2\sin2(\theta_0+q) = m_0\ell g q\cos\theta_0 - m_0\ell^2(\omega_0 p\sin2\theta_0 + \omega_0^2 q\cos2\theta_0) + \text{H.O.T.} \tag{22}$$

In Eq. (22) the terms $m_0\ell g q\cos\theta_0 - m_0\ell^2\omega_0^2 q\cos2\theta_0$ can be further simplified to be

$$m_0\ell(gq\cos\theta_0 - \ell\omega_0^2 q\cos2\theta_0) = m_0\ell(gq\cos\theta_0 - \ell\omega_0^2 q(\cos^2\theta_0 - \sin^2\theta_0)) = m_0\ell^2\omega_0^2 q\sin^2\theta_0, \tag{23}$$

where $gq\cos\theta_0 - \ell\omega_0^2 q\cos^2\theta_0$ were canceled using Eq. (11).

Substituting Eqs. (22) and (23) back into Eq. (18) and dropping H.O.T. lead to

$$m_0(\ell^2+\tfrac{2}{5}r^2)\,\ddot{q} + m_0\ell^2\omega_0^2\sin^2\theta_0 q - m_0\ell^2\omega_0\sin2\theta_0\, p + b_0\dot{q} = 0. \tag{24}$$

For Eq. (19), the nonlinear terms can each be expressed to be

$$\dot{p}\sin^2(\theta_0+q) = \dot{p}\sin^2\theta_0 + \text{H.O.T.}, \tag{25}$$

$$(\omega_0+p)\dot{q}\sin2(\theta_0+q) = \omega_0\dot{q}\sin2\theta_0 + \text{H.O.T.}, \tag{26}$$

where H.O.T. denotes terms associated with $\dot{p}q$, $p\dot{q}$, q^2 and other higher-order products.

Substituting Eqs. (25) and (26) back into Eq. (19) and dropping H.O.T. yield

$$m_0\left(\ell^2\sin^2\theta_0 + \tfrac{2}{5}r^2\right)\dot{p} + m_0\ell^2\omega_0\sin2\theta_0\,\dot{q} + b_1 p = v. \tag{27}$$

Eqs. (24) and (27) are therefore the linearized equations of Eqs. (7) and (8) about the equilibrium angle θ_0 and equilibrium rotational speed ω_0. Note that $\sin\theta_0$ and $\sin2\theta_0$ can be expressed in terms of ω_0 using Eq. (12):

$$\sin\theta_0 = \sqrt{1-\cos^2\theta_0} = \sqrt{1-\left(\frac{g}{\ell\omega_0^2}\right)^2}, \tag{28}$$

$$\sin2\theta_0 = 2\sin\theta_0\cos\theta_0 = 2\sqrt{1-\left(\frac{g}{\ell\omega_0^2}\right)^2}\,\frac{g}{\ell\omega_0^2}. \tag{29}$$

Transfer function: The transfer function between vertical oscillations and the excitation torque can be derived by taking Laplace transform on Eqs. (24) and (27).

From Eq. (24),

$$\frac{p}{q}(s) = \frac{m_0(\ell^2+\frac{2}{5}r^2)s^2 + b_0 s + m_0\ell^2\omega_0^2\sin^2\theta_0}{m_0\ell^2\omega_0\sin2\theta_0}. \tag{30}$$

Substitution of the above equation into Eq. (27) leads to

$$\frac{q}{v}(s) = \frac{m_0\ell^2\omega_0\sin2\theta_0}{d_3s^3 + d_2s^2 + d_1s + d_0}, \tag{31}$$

where

$$d_3 = m_0^2(\ell^2\sin^2\theta_0 + \tfrac{2}{5}r^2)(\ell^2+\tfrac{2}{5}r^2), \tag{32}$$

$$d_2 = m_0 b_0(\ell^2\sin^2\theta_0 + \tfrac{2}{5}r^2) + m_0 b_1(\ell^2+\tfrac{2}{5}r^2), \tag{33}$$

$$d_1 = m_0^2(\ell^2\sin^2\theta_0 + \tfrac{2}{5}r^2)\ell^2\omega_0^2\sin^2\theta_0 + m_0^2(\ell^2\omega_0\sin2\theta_0)^2 + b_0 b_1, \tag{34}$$

$$d_0 = m_0 b_1\ell^2\omega_0^2\sin^2\theta_0. \tag{35}$$

The axial force exerted on the support (referring to Fig. 2) can be expressed to be

$$F_Z = m_0\ell\ddot{q}\sin\theta_0. \tag{36}$$

Note that the nonlinear term, $m_0\ell\dot{q}^2\cos\theta_0$, has been dropped.

From Eqs. (36) and (31)

$$\frac{F_Z\ell}{v}s = \frac{m_0^2\ell^4\omega_0\sin2\theta_0\sin\theta_0 s^2}{d_3s^3 + d_2s^2 + d_1s + d_0}. \tag{37}$$

Note that $F_Z\ell/v$ is a dimensionless group. Denote the excitation frequency in radian per second to be ω, and define the *normalized* frequency $\hat{\omega}$ (also a dimensionless group) to be

$$\hat{\omega} = \frac{\omega}{\sqrt{g/\ell}}. \tag{38}$$

It will be shown that the normalized frequency response, $(F_Z\ell/v)(j\hat{\omega})$, is dependent on the four dimensionless groups defined below:

$$\hat{\omega}_0 = \frac{\omega_0}{\sqrt{g/\ell}}, \tag{39}$$

$$\hat{r} = r/\ell, \tag{40}$$

$$\hat{b}_0 = \frac{b_0}{m_0\ell\sqrt{\ell g}}, \tag{41}$$

$$\hat{b}_1 = \frac{b_1}{m_0\ell\sqrt{\ell g}}. \tag{42}$$

Substituting s by $j\omega$ in Eq. (37) we have

$$\frac{F_Z\ell}{v}(j\omega) = \frac{-m_0^2\ell^4\omega_0 \sin 2\theta_0 \sin\theta_0\omega^2}{j(-d_3\omega^3 + d_1\omega) - d_2\omega^2 + d_0}. \tag{43}$$

Divide both the numerator and the denominator of Eq. (43) by $m_0^2 g\ell^2\sqrt{g\ell}$ and we have

$$\frac{F_Z\ell}{v}(j\hat{\omega}) = \frac{-\hat{\omega}_0 \sin 2\theta_0 \sin\theta_0\hat{\omega}^2}{j(-\hat{d}_3\hat{\omega}^3 + \hat{d}_1\hat{\omega}) - \hat{d}_2\hat{\omega}^2 + \hat{d}_0}, \tag{44}$$

where

$$\hat{d}_3 = (\sin^2\theta_0 + \tfrac{2}{5}\hat{r}^2)(1 + \tfrac{2}{5}\hat{r}^2), \tag{45}$$

$$\hat{d}_2 = \hat{b}_0(\sin^2\theta_0 + \tfrac{2}{5}\hat{r}^2) + \hat{b}_1(1 + \tfrac{2}{5}\hat{r}^2), \tag{46}$$

$$\hat{d}_1 = (\sin^2\theta_0 + \tfrac{2}{5}\hat{r}^2)\hat{\omega}_0^2 \sin^2\theta_0 + \hat{\omega}_0^2 \sin^2 2\theta_0 + \hat{b}_0\hat{b}_1, \tag{47}$$

$$\hat{d}_0 = \hat{b}_1\hat{\omega}_0^2 \sin^2\theta_0. \tag{48}$$

Since $\sin\theta_0$ and $\sin 2\theta_0$ can be expressed in term of $\hat{\omega}_0$ (Eqs. (28) and (29)), it is verified from Eqs. (44)–(48) that $(F_Z\ell/v)(j\hat{\omega})$ is indeed determined by the four independent groups defined in Eqs. (39) and (42).

Figs. 4 and 5 show a set of response curves for $\hat{r} = 0$ and with $\hat{\omega}_0$ varying from 2 to 4. In Fig. 4, $\hat{b}_1$ is 0.1 and the responses with $\hat{b}_0 = 0.1, 0.3, 1, 3$ are compared. In Fig. 5, $\hat{b}_0$ is fixed at 0.1 and the responses with $\hat{b}_1 = 0.1, 1, 2, 5$ are compared. Note that in practice the rotational damping associated with an electric motor may not be neglected due to the motor's back electromotive force (back emf), which adds to the effective damping when operated in voltage mode. By comparing Figs. 4 and 5 it can be seen that, unlike vertical damping coefficient $\hat{b}_0$, which has about the same effect for all rotational speeds, the rotational damping coefficient $\hat{b}_1$ affects the response significantly when the rotational speed is low, but has diminishing effect on vertical oscillations for higher-speed rotations. Physically this is because vertical vibrations are induced by variations in the rotational speed. At high excitation frequencies the speed variations are dominated by the inertia of the arm; that is, the inertia force (torque) is more significant than the damping force (torque) at high frequencies (refer to Eq. (27)). Fig. 6 shows the cross effect of vertical damping and rotational damping by varying $\hat{b}_0$ from 0.1 to 1 with $\hat{b}_1$ set first to be 0.1 and then 3, for a rotational speed of $\hat{\omega}_0 = 3$.

Fig. 7 shows the effect of $\hat{r}$ on the frequency response by comparing the curves with $\hat{r} = 0, 0.4$ and 0.8. It is seen that the resonant frequency decreases with $\hat{r}$. This can be explained by the fact that, for a solid ball of mass m_0, the rotational inertia increases with the radius of the ball, and natural frequency decreases as inertia increases.

From Figs. 4 and 5 it is seen that given an excitation frequency, the magnitude of response is substantially affected by the rotational speed. To achieve maximum output to input ratio, the rotational speed should be adjusted in such a way that the resonant (natural) frequency of vertical oscillations is close to the excitation frequency. A detailed examination on the natural frequency is in order.

Natural frequencies of vertical oscillations: Given a rotational speed, the natural frequency of vertical oscillations (denoted by ω_n) can be determined from the undamped dynamic equations. Setting $\hat{b}_0 = \hat{b}_1 = 0$ in Eqs. (45)–(48), we have

$$\hat{d}_3 = (\sin^2\theta_0 + \tfrac{2}{5}\hat{r}^2)(1 + \tfrac{2}{5}\hat{r}^2), \tag{49}$$

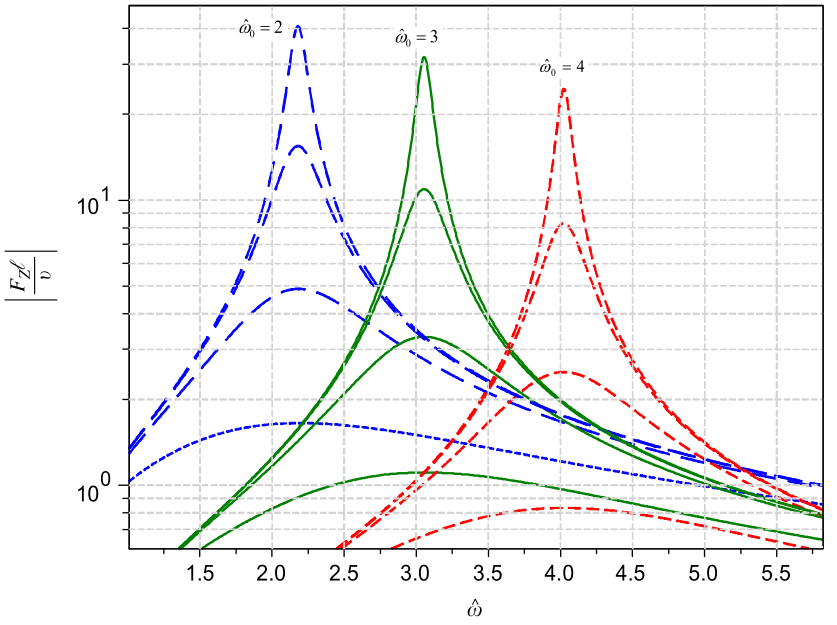

Fig. 4. Frequency responses for $\hat{\omega}_0 = 2,3,4$ with $\hat{b}_0 = 0.1,0.3,1,3$ ($\hat{b}_1 = 0.1$).

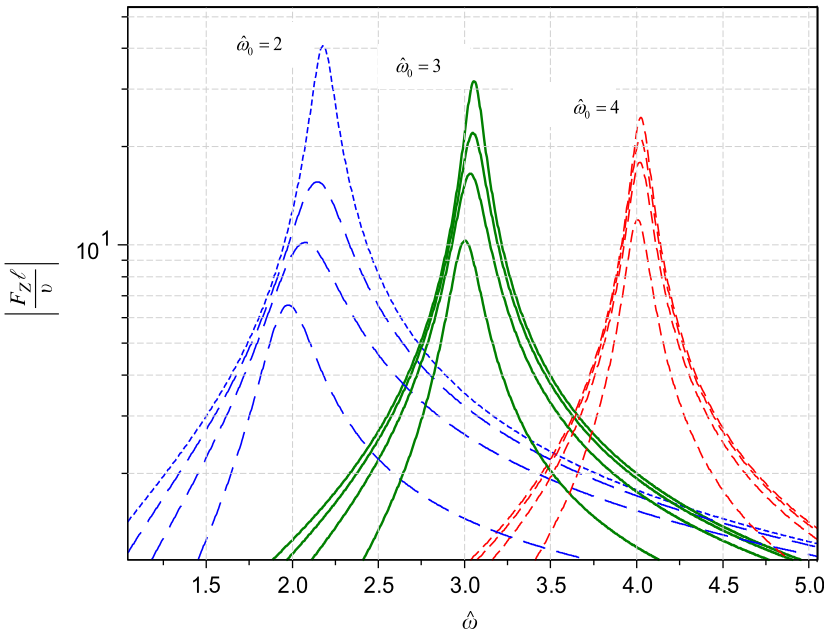

Fig. 5. Frequency responses for $\hat{\omega}_0 = 2,3,4$ with $\hat{b}_1 = 0.1,1,2,5$ ($\hat{b}_0 = 0.1$).

$$\hat{d}_2 = 0, \tag{50}$$

$$\hat{d}_1 = (\sin^2\theta_0 + \tfrac{2}{5}\hat{r}^2)\hat{\omega}_0^2 \sin^2\theta_0 + \hat{\omega}_0^2 \sin^2 2\theta_0, \tag{51}$$

$$\hat{d}_0 = 0, \tag{52}$$

and Eq. (44) is reduced to

$$\frac{F_Z \ell}{V}(j\hat{\omega}) = \frac{-j\hat{\omega}_0 \sin 2\theta_0 \sin\theta_0\, \hat{\omega}}{(\sin^2\theta_0 + \frac{2}{5}\hat{r}^2)(1+\frac{2}{5}\hat{r}^2)\hat{\omega}^2 - ((\sin^2\theta_0 + \frac{2}{5}\hat{r}^2)\sin^2\theta_0 + \sin^2 2\theta_0)\hat{\omega}_0^2}. \tag{53}$$

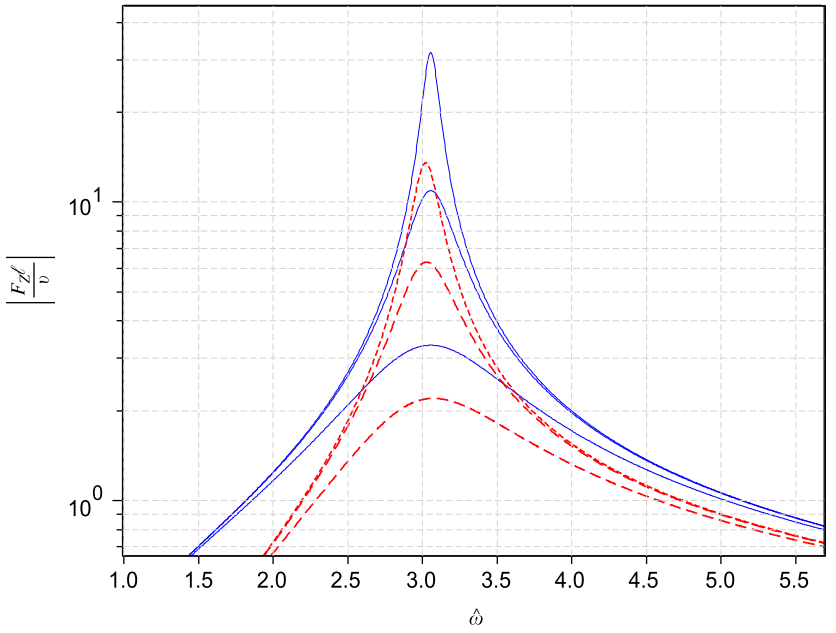

Fig. 6. Frequency responses for $\hat{b}_0 = 0.1, 0.3, 1$ with $\hat{b}_1 = 0.1$ (solid curves) and $\hat{b}_1 = 3$ (dashed curves) ($\hat{\omega}_0 = 3$).

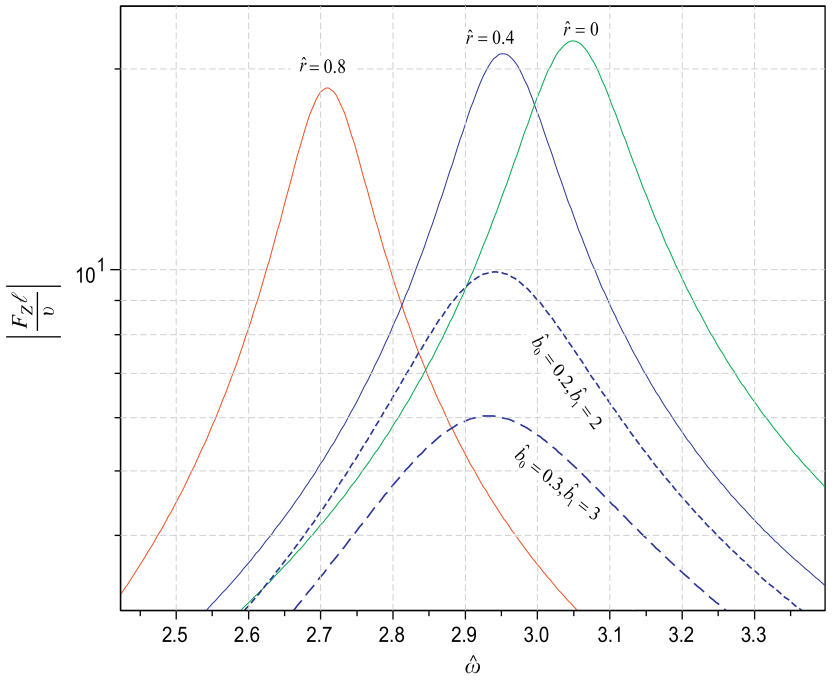

Fig. 7. Frequency responses for $\hat{r} = 0, 0.4$ and 0.8, with $\hat{\omega}_0 = 3$ and $\hat{b}_0 = 0.1, \hat{b}_1 = 1$ (solid curves); the dashed curves are for $\hat{r} = 0.4$ with higher damping coefficients (as indicated).

Define the *normalized* natural frequency $\hat{\omega}_n$ to be

$$\hat{\omega}_n = \frac{\omega_n}{\sqrt{g/\ell}}. \tag{54}$$

From Eq. (53) we have

$$\hat{\omega}_n^2 = \frac{(\sin^2\theta_0 + \frac{2}{5}\hat{r}^2)\sin^2\theta_0 + \sin^2 2\theta_0}{(1+\frac{2}{5}\hat{r}^2)(\sin^2\theta_0 + \frac{2}{5}\hat{r}^2)}\hat{\omega}_0^2. \tag{55}$$

As a confirmation of the above derivation, the natural frequency can be alternatively obtained from Eqs. (24) and (27) directly. Setting ν=0 and dropping the term associated with damping ($b_1\ p$) in Eq. (27), we have

$$p = -\frac{\ell^2\omega_0 \sin 2\theta_0}{\ell^2 \sin^2\theta_0 + \frac{2}{5}r^2} q. \tag{56}$$

Substitution of Eq. (56) into Eq. (24) leads to

$$\left(\ell^2 + \frac{2}{5}r^2\right)\ddot{q} + \left(\ell^2\omega_0^2 \sin^2\theta_0 + \frac{(\ell^2\omega_0 \sin 2\theta_0)^2}{\ell^2 \sin^2\theta_0 + \frac{2}{5}r^2}\right) q = 0, \tag{57}$$

where the damping term ($b_0\dot{q}$) has been dropped. From the last equation the natural frequency is obtained to be

$$\omega_n^2 = \frac{(\ell^2 \sin^2\theta_0 + \frac{2}{5}r^2)(\ell \sin\theta_0)^2 + (\ell^2 \sin 2\theta_0)^2}{(\ell^2 + \frac{2}{5}r^2)(\ell^2 \sin^2\theta_0 + \frac{2}{5}r^2)}\ \omega_0^2. \tag{58}$$

Divide the denominator and the numerator of Eq. (58) both by ℓ^4, then divide both sides of the equation by g/ℓ, and we reach Eq. (55). This confirms the previous derivation.

If the radius of the solid ball is negligible compared to the link's length, i.e., $\hat{r} = 0$, from Eq. (55) the natural frequency can be simplified to be

$$\hat{\omega}_n^2 = \hat{\omega}_0^2(\sin^2\theta_0 + \sin^2 2\theta_0) = \hat{\omega}_0^2(1 + 3\cos^2\theta_0) = \hat{\omega}_0^2 + \frac{3}{\hat{\omega}_0^2}, \tag{59}$$

where the identity $\cos^2\theta_0 = 1/\hat{\omega}_0^4$ (from Eq. (12)) has been used.

Fig. 8 shows the curves relating $\hat{\omega}_n$ to $\hat{\omega}_0$ for $\hat{r}$ varying from 0 to 0.9. In general the natural frequency increases with the rotational speed. For small $\hat{r}$ ($\hat{r} < 0.35$), however, the curves move downward initially and then upward as $\hat{\omega}_0$ increases beyond certain values. The concavity is most significant when $\hat{r} = 0$, for which we have the following observations from Eq. (59):

(i) $\hat{\omega}_n$ decreases with $\hat{\omega}_0$ for $1 < \hat{\omega}_0^2 < \sqrt{3}$.
(ii) $\hat{\omega}_n$ increases with $\hat{\omega}_0$ for $\hat{\omega}_0^2 > \sqrt{3}$.
(iii) $\hat{\omega}_n \approx \hat{\omega}_0$ if $\hat{\omega}_0 \gg 1$.

Note that (i) and (ii) can be verified by differentiating $\hat{\omega}_n^2$ with respect to $\hat{\omega}_0^2$. From the above observations and in view of Fig. 8, the natural frequency increases monotonically with the rotational speed if $\hat{\omega}_0^2 > \sqrt{3}$, which is a *sufficient* condition for all $\hat{r}$'s.

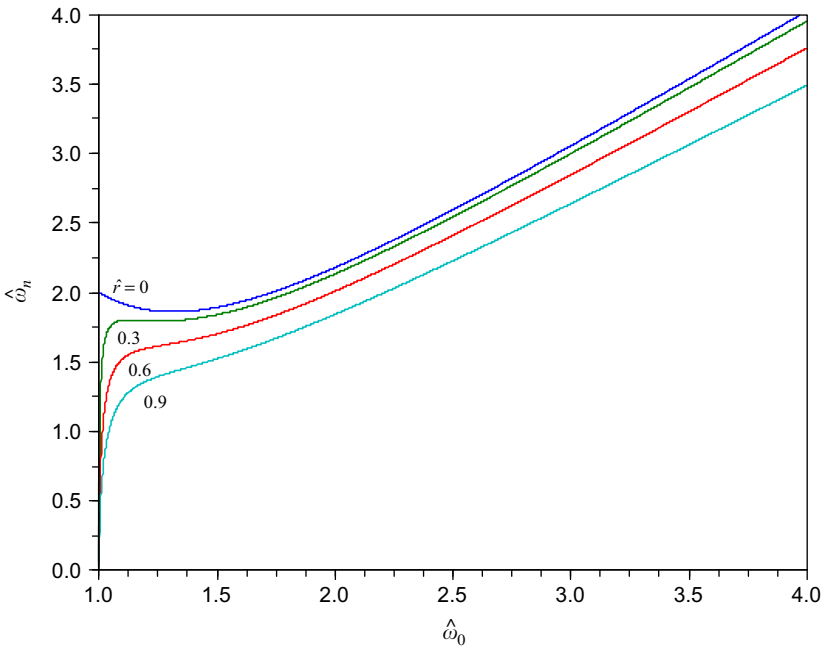

Fig. 8. Vertical natural frequency versus rotational speed for $\hat{r} = 0, 0.3, 0.6$ and 0.9.

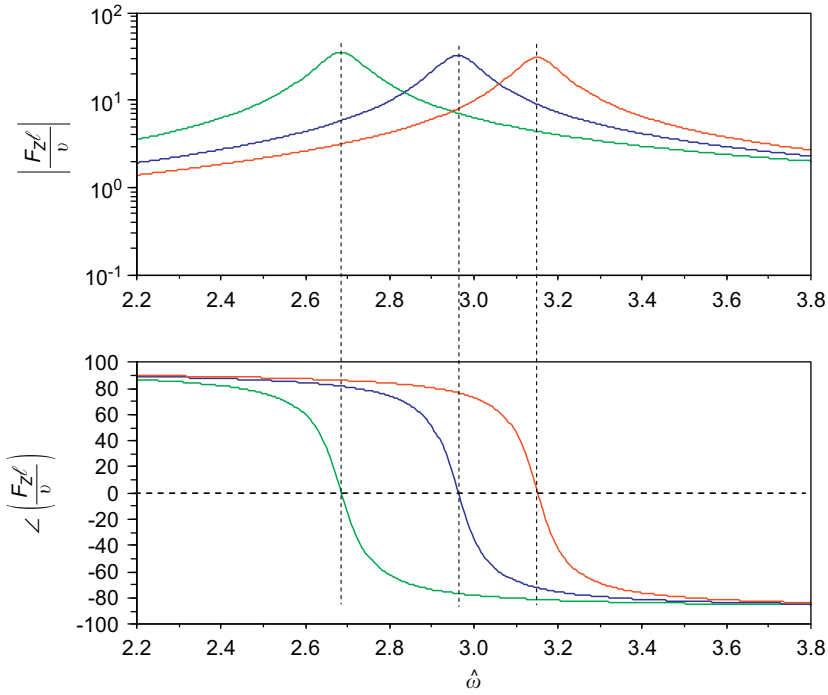

Fig. 9. Phase-frequency relations: at resonance, the vertical oscillation force is in phase with the excitation torque (the phase angle is 0).

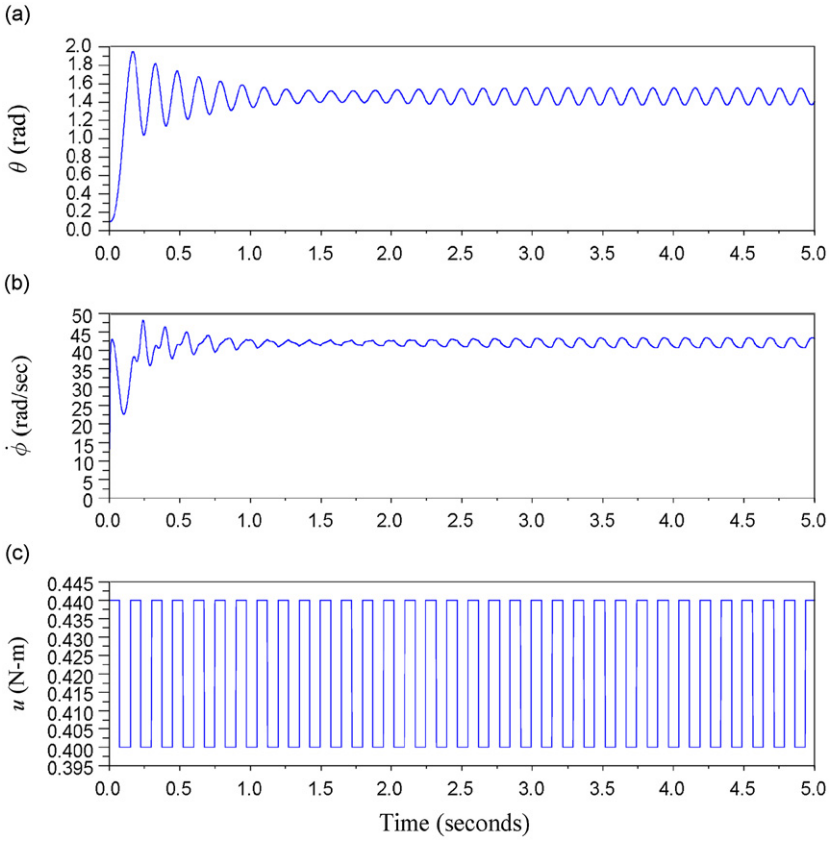

Fig. 10. Time response with a square-wave input: (a) vertical angle; (b) rotational speed; and (c) input torque.

Resonance detection by phase angles: Besides rotational speeds, the natural frequency of vertical oscillations is also affected by the configuration of the rotational arm such as the radius of the ball. In practice it may not be precisely calculated in advance. However, by studying the phase-frequency relationship (Fig. 9), we find that at resonance the output signal is *in phase* with the excitation input. Since the resonance frequency is sensitive to the rotational speed, it can be tuned by adjusting the speed according to the phase angle between input and output. This issue will be elaborated further in the next section.

4. Simulation of the nonlinear system

Excitation on the original nonlinear system (Eqs. (7)–(8)) will be performed via numerical simulation with a simple square-wave input, as is practically done in motor control. Since the nominal speed of rotation is proportional to the level (or mean) of the square input, it will be observed how the response is sensitive to the level of input.

The parameters of the rotational arm used in the simulations are as follows: m_0=0.2 kg, $\ell = 0.05$ m, r=0.02 m, $b_0 = 7 \times 10^{-4}$ N m s and $b_1 = 1 \times 10^{-2}$ N m s. (Note that $\hat{b}_0 = 0.1, \hat{b}_1 = 1.43$ from Eqs. (41) and (42).) The excitation frequency is set at 42 rad/s, to which the corresponding normalized frequency ($\hat{\omega}$) can be calculated to be

$$\hat{\omega} = \frac{42}{\sqrt{9.8/0.05}} = 3. \tag{60}$$

It will be examined how the response is affected by different rotational speeds given this excitation frequency.

Fig. 10 shows the time response with a square-wave input shown in Fig. 10c. The closeup view at steady state is shown in Fig. 11. Since the mean value of input is 0.42, the average rotational speed is 42 rad/s (=0.42/0.01). (Note that the average rotational speed, ω_0, is equal to the mean value of u divided by b_1.)

In Fig. 12, the level of input is shifted from 0.28 (Curve 1), to 0.42 (Curve 2), and finally to 0.56 (Curve 3) while the peak-to-peak value of the input waveform is kept unchanged. The average rotational speed is therefore shifted from 28, to 42, and then to 56 rad/s, corresponding to $\hat{\omega}_0 = 2$, 3, and 4, respectively. From Eqs. (12) and (55) the (normalized) natural frequency of vertical vibrations for $\hat{\omega}_0 = 3$ and $\hat{r} = 0.4 (= r/\ell)$ is 2.96, which is close to the excitation frequency. Consequently it is seen that Curve 2 has by far the largest magnitude compared to the under-driven and over-driven cases

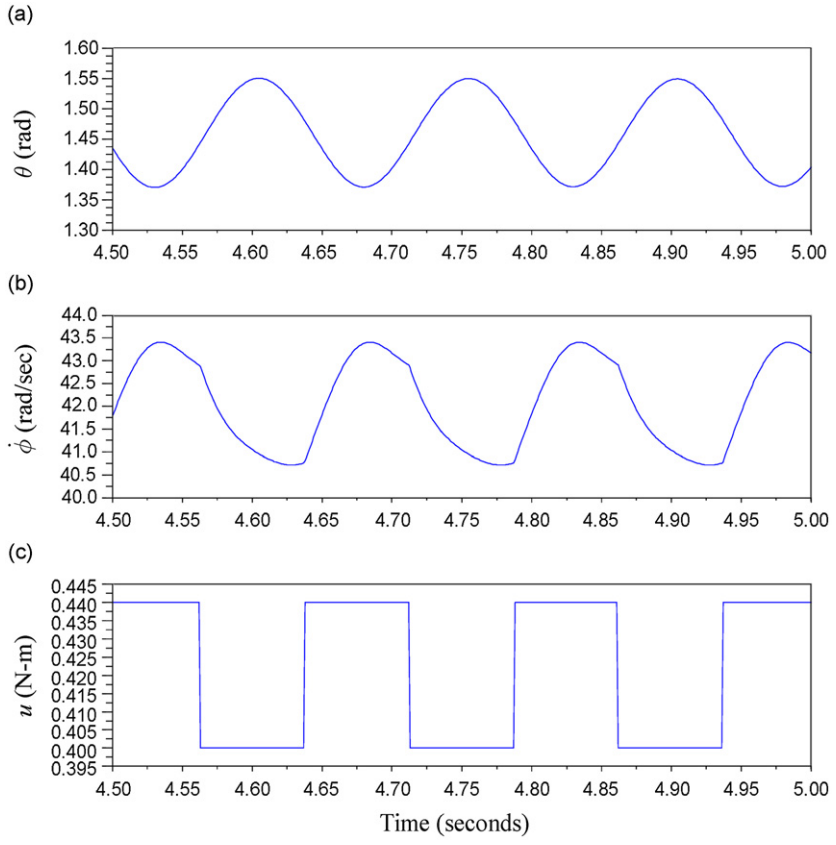

Fig. 11. Closeup view for the time response of the previous figure. Note that the vertical oscillations (θ) are near sinusoidal even though variations in the rotational speed are not.

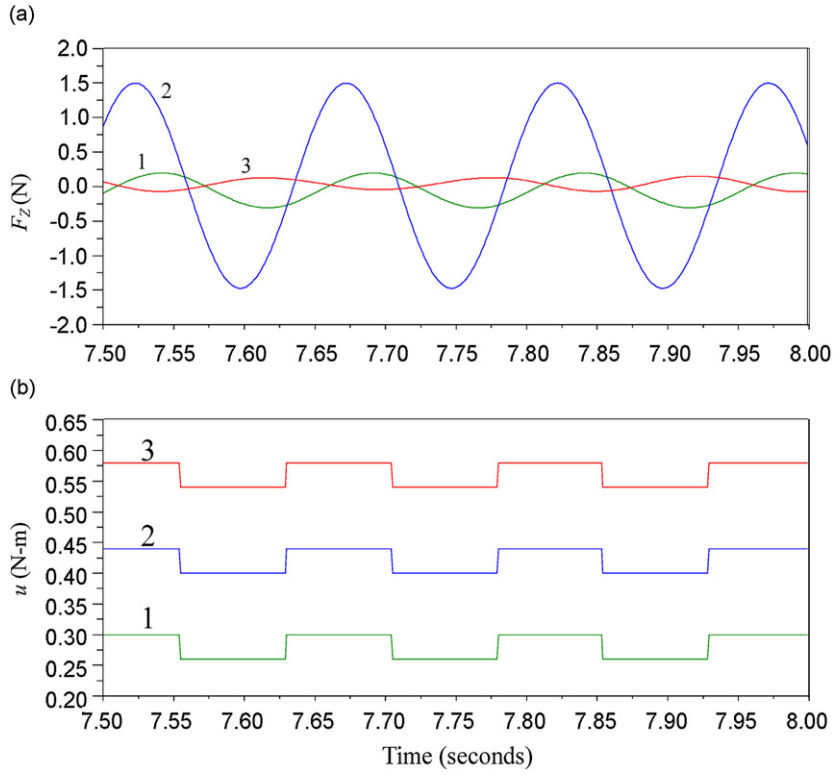

Fig. 12. Vertical-force responses (a) for various levels of input (b). When the level of input is such that $\omega_0 = 42$ rad/s (Curve 2), the resonant frequency (almost) matches the excitation frequency, resulting in maximum magnitude of response.

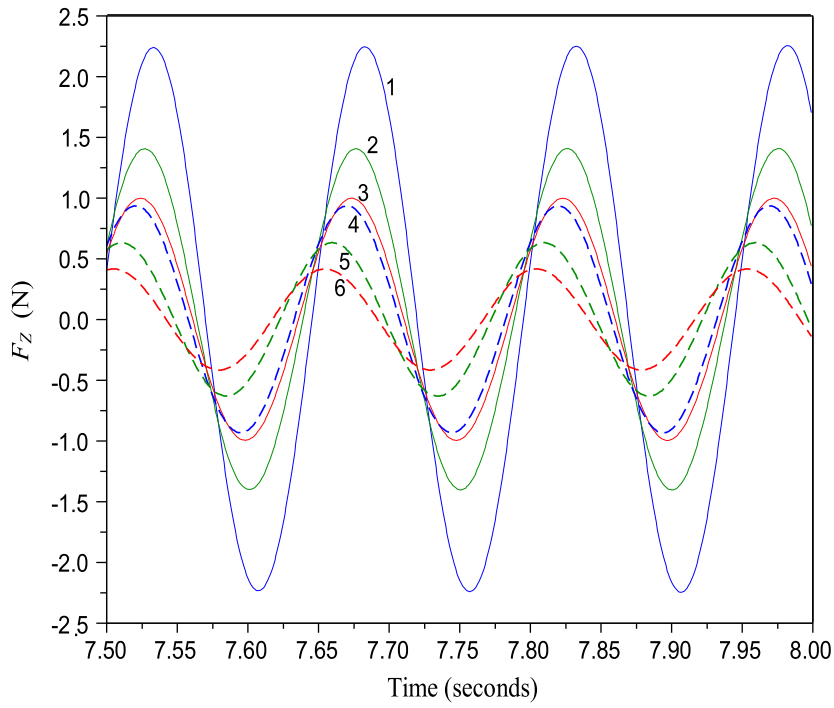

Fig. 13. Vertical-force responses for ω_0 set to be 42 rad/s, with $\hat{b}_0$ varying from 0.1 to 0.3 (solid curves) and $\hat{b}_1$ from 0.1 to 5 (dashed curves): (1) $\hat{b}_0 = \hat{b}_1 = 0.1$; (2) $\hat{b}_0 = 0.2$, $\hat{b}_1 = 0.1$; (3) $\hat{b}_0 = 0.3$, $\hat{b}_1 = 0.1$; (4) $\hat{b}_0 = 0.3$, $\hat{b}_1 = 0.5$; (5) $\hat{b}_0 = 0.3$, $\hat{b}_1 = 2.5$; and (6) $\hat{b}_0 = 0.3$, $\hat{b}_1 = 5$.

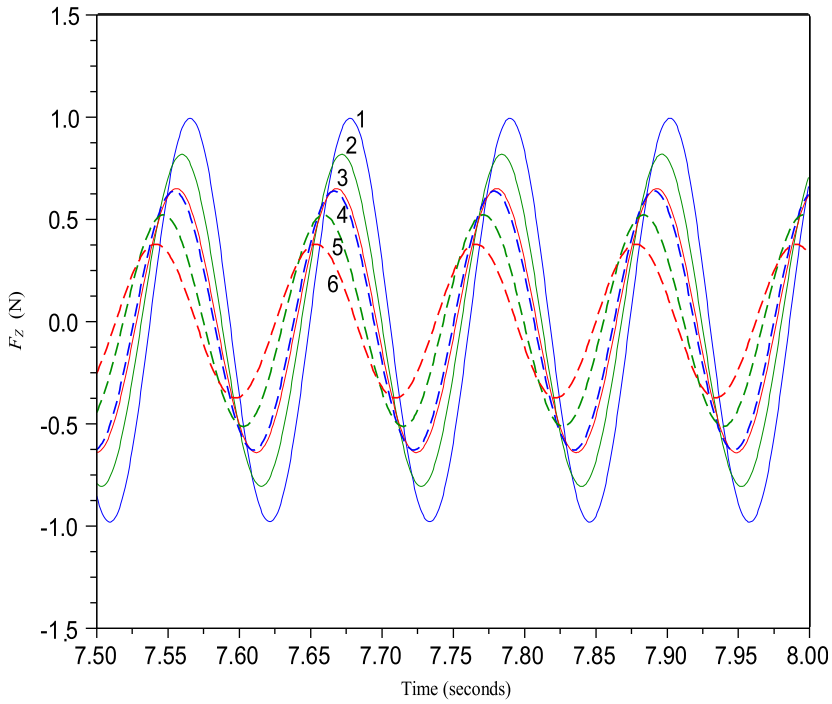

Fig. 14. Vertical-force responses for ω_0 set to be 56 rad/s, with $\hat{b}_0$ varying from 0.1 to 0.3 (solid curves) and $\hat{b}_1$ from 0.1 to 5 (dashed curves): (1) $\hat{b}_0 = \hat{b}_1 = 0.1$; (2) $\hat{b}_0 = 0.2$, $\hat{b}_1 = 0.1$; (3) $\hat{b}_0 = 0.3$, $\hat{b}_1 = 0.1$; (4) $\hat{b}_0 = 0.3$, $\hat{b}_1 = 0.5$; (5) $\hat{b}_0 = 0.3$, $\hat{b}_1 = 2.5$; and (6) $\hat{b}_0 = 0.3$, $\hat{b}_1 = 5$.

(Curves 1 and 3). Also notable in Fig. 12 is that the output signal lags the input when the input's level is lower than the target (Curve 1), while the output leads the input when the input's level is higher (Curve 3). The result is consistent with the frequency response of Fig. 9. This property is significant because it indicates that the level of input can be adjusted upward or downward according to the measured phase angle in order to yield the strongest shaking force.

To observe the damping effects on the time response, b_0 and b_1 are varied over a certain range given a nominal rotational speed. Fig. 13 shows the vertical force response for $\omega_0 = 42$ rad/s (such that $\hat{\omega}_0 = 3$) with $\hat{b}_0$ varying from 0.1 to 0.3 and $\hat{b}_1$ from 0.1 to 5. In Fig. 14 the rotational speed is raised to be 56 rad/s ($\hat{\omega}_0 = 4$). These figures confirm previous observations in the frequency response that vertical vibrations are more sensitive to the magnitude of vertical damping. Besides, the rotational damping has diminishing effect on vertical vibrations as the rotational speed increases. Note, however, with higher rotational damping the level of control input must be raised accordingly in order to maintain the same rotational speed.

5. Conclusion

It was shown that 3-D vibrations can be generated by applying an input torque to a single axis of rotation. The input signal contains two components: a constant level that maintains the average speed of the eccentric weight at a desired value that results in lateral vibrations, and a fluctuating torque to excite vertical oscillations. From the frequency response it was seen that the magnitude of vertical oscillations is significantly affected by the level of the rotational speed. That is because vertical natural frequencies are dependent on the speed of rotation. This vibration generator may therefore be operable over a wide range of frequencies by varying the rotational speed according to the excitation frequency. The performance was confirmed by numerical simulations on the original nonlinear system.

The length of eccentricity (i.e., length of the rotational arm) may be reduced or extended according to the desired frequency range: the higher the frequency, the shorter the length. This mechanism may be used in vibratory feeders for generation of helical vibrations. It may also be used as a haptic feedback device to provide sophisticated vibrotactile signals.

References

[1] J. Ryu, J. Jung, S. Kim, S. Choi, Perceptually transparent vibration rendering using a vibration motor for haptic interaction, *Proceedings of the 16th IEEE International Conference on Robot & Human Interactive Communication*, Jeju, Korea, 2007, pp. 310–315.

[2] S. Kim, G. Park, S. Yim, S. Choi, S. Choi, Gesture-recognizing hand-held interface with vibrotactile feedback for 3D interaction, *IEEE Transactions on Consumer Electronics* 55 (3) (2009) 1169–1177.
[3] V. Hayward, O.R. Astley, M. Cruz-Hernandez, D. Grant, G. Robles-De-La-Torre, Haptic interfaces and devices, *Sensor Review* 24 (1) (2004) 16–29.
[4] A. Halmai, A. Lukacs, New linear-electromagnetic actuator used for cellular phones, *Periodica Polytechnica, Mechanical Engineering* 51 (1) (2007) 19–22.
[5] S.M. Golaszewski, F. Zschiegner, C.M. Siedentopf, J. Unterrainer, R.A. Sweeney, W. Eisnerf, S. Lechner-Steinleitner, F.M. Mottaghyg, S. Felber, A new pneumatic vibrator for functional magnetic resonance imaging of the human sensorimotor cortex, *Neuroscience Letters* 324 (2002) 125–128.
[6] G. Boothroyd, *Assembly Automation and Product Design*, second ed., Taylor and Francis, Boca Raton, Florida, 2005.
[7] G.P. Maul, M.B. Thomas, A systems model and simulation of the vibratory bowl feeder, *Journal of Manufacturing Systems* 16 (5) (1997) 309–314.
[8] R.-P. Berretty, K. Goldberg, M.H. Overmars, A.F. Van der Stappen, Trap design for vibratory bowl feeders, *The International Journal of Robotics Research* 20 (11) (2001) 891–908.
[9] A. Mitani, N. Sugano, S. Hirai, Micro-parts feeding by a saw-tooth surface, *IEEE/ASME Transactions on Mechatronics* 11 (6) (2006) 671–681.
[10] M.C. Fuerstenau, K.N. Han (Eds.), *Principle of Mineral Processing*, Society for Mining Metallurgy & Exploration, Littleton, Colorado, 2003, pp. 400–406.
[11] J.A. Vilan Vilan, A. Segade Robleda, P.J. Garcia Nieto, C. Casqueiro Placer, Approximation to the dynamics of transported parts in a vibratory bowl feeder, *Mechanism and Machine Theory* 44 (2009) 2217–2235.
[12] H.V. Thomas, P. Umbanhowar, K.M. Lynch, Friction-induced velocity fields for point parts sliding on a rigid oscillated plate, *The International Journal of Robotics Research* 28 (8) (2009) 1020–1039.
[13] M. Ramalingam, G.L. Samuel, Investigation on the conveying velocity of a linear vibratory feeder while handling bulk-sized small parts, *The International Journal of Advanced Manufacturing* 44 (3–4) (2009) 372–382.
[14] P.C.-P. Chao, C.-Y. Shen, Dynamic modeling and experimental verification of a piezoelectric part feeder in a structure with parallel bimorph beams, *Ultrasonics* 46 (2007) 205–218.
[15] S.B. Choi, D.H. Lee, Modal analysis and control of a bowl parts feeder activated by piezoceramic actuators, *Journal of Sound and Vibration* 275 (2004) 452–458.
[16] S.-T. Wu, Active pendulum vibration absorbers with a spinning support, *Journal of Sound and Vibration* 323 (2009) 1–16.